Influence of the sedimentary environment of the Wufeng-Longmaxi shale on organic matter accumulation in the Dingshan area, Sichuan Basin

Qiang Wang, Yue Feng*, Ping Gao, Guangming Meng, Chengang Lu, Qizhang Fan, Gang Li, Yineng Tan and Xianming Xiao

School of Energy Resources, China University of Geosciences (Beijing), Beijing, China

The sedimentary environment and organic matter (OM) accumulation are vital indicators for shale gas exploration. However, research on deep shale gas systems is relatively limited; moreover, the exploration of deep shale gas in the southeastern Sichuan Basin has entered a period of stagnation. In this study, systematic geochemical analysis of Wufeng (WF) and the first member of the Longmaxi (Long-1) deep shale samples from the recently drilled DY7 well in the Dingshan area of the Sichuan Basin is carried out, and the longitudinal variations in major and trace elements are revealed. The differences in the WF, lower section of the Long-1 (Long-1_1) and upper section of the Long-1 (Long-1_2) shales are studied in terms of redox conditions, paleoproductivity, terrigenous detrital input, sedimentation rate and paleoclimate, and the different main controlling factors of OM accumulation for these three layers are discussed. The WF shale has a higher TOC content (mean: 5.73%), the Long-1_1 shale has a high TOC content (mean: 2.89%), while the Long-1_2 shale has a low TOC content (mean: 1.44%). For the WF shale, due to complex geological events and large fluctuations in element contents, its TOC content is poorly correlated with these indices, redox and paleoproductivity proxies have a positive association with the Long-1_1 shale's TOC content, but negatively correlated with terrigenous input and sedimentation rate indices. The formation of these two sets of organic-rich shales (TOC > 2%) is jointly controlled by good preservation conditions. In contrast, the TOC content of the WF shale is higher than that of the Long-1_1 shale as the result that terrigenous input and sedimentation rate of the Long-1_1 shale represent the dilution and destruction of OM, which is different from the former. During the Long-1_2 depositional period, the water column experienced weak reducing conditions and low productivity, and its high terrigenous debris input further diluted the OM, leading to a low TOC content.

KEYWORDS

Sichuan Basin, Wufeng-Longmaxi formation, deep shale, sedimentary environment, organic matter accumulation

1 Introduction

In recent years, shale oil and gas have received extensive attention (Liu et al., 2021a; Feng et al., 2021; Wang E. Z. et al., 2022; Feng et al., 2023b; Lu et al., 2023; Wang et al., 2023; Hu et al., 2024; Meng et al., 2024), especially in the Wufeng-Longmaxi (WF-LMX) Formation (Guo et al., 2020; Ma et al., 2020; Ma et al., 2021). According to its lithofacies characteristics and reservoir physical properties, the WF-LMX shale is generally divided into upper and lower sets of reservoirs (Shu et al., 2020; Shu and Wang, 2021). The Long-1_2 shale has poor reservoir physical properties, while the Long-1_1 and WF shales have good physical properties. The middle-shallow (<3,500 m) shale gas reservoirs (e.g., the Jiaoshiba area) experienced large-scale commercial development. In the past 5 years, shale gas exploration in the Sichuan Basin has expanded to deeper depths (>3,500 m). Important progress has been made in the Dingshan, Yongchuan, and Luzhou blocks, with multiple wells yielding high production, indicating that the deep WF-LMX shale plays a crucial role in the shale gas supply (Wang et al., 2016; Nie et al., 2023). The study shows that middle-shallow shale gas, covers an area of about 6.3×10^4 km^2, while deep shale is about 12.6×10^4 km^2. Moreover, it is estimated that the amount of deep shale resources is approximately twice that of middle-shallow shale (He et al., 2021). Deep shale gas has been tested in areas such as Weiyuan, Yongchuan, Changning, Luzhou, Dingshan, and Dongxi, and many high-yield shale gas wells have been discovered (e.g., Well DY4, 3HF, L203, and Yang 101H2-8) (Guo et al., 2020; Zou et al., 2021). However, compared with those on middle-shallow shale reservoirs, only a few systematic studies have been performed on deep shale, and there are differences in the understanding of geological factors related to reservoir quality (Wang et al., 2019; Ma et al., 2021; Meng et al., 2022; Feng et al., 2023a; Feng et al., 2024).

Previous studies have reported that the high yield of shale gas is closely related to the organic matter accumulation (OMA) (Li et al., 2019; Ma et al., 2020; Lu et al., 2024). The sedimentary environment is a crucial factor for determining the quality of shale and is related to the material basis of shale gas generation and storage. Geochemical parameters are among the most used methods for reconstructing the paleoenvironment and exploring the driving mechanism for OMA (Liu et al., 2017; Zhang et al., 2022; Zhang et al., 2023; Lu et al., 2024). Previous studies have shown that basin confinement creates readily stratified sedimentary waters; in the case of anoxic environments, OM could be enriched in large quantities even if paleoproductivity is low (Algeo and Rowe, 2012). Pedersen and Calvert. (1990) believed that paleoproductivity plays a key role in OMA. In addition, Ma et al. (2020) proposed that organic-rich shale can form even in oxidized water bodies, e.g., the LMX shale in the Weiyuan and Changning areas. Moreover, two ways in which terrigenous debris input can impact OMA are (a) by controlling the rate of OM burial and deposition, and (b) by altering the conditions of OM in the ocean (Zhang et al., 2023). Specifically, Adams et al. (2010) suggested that the input of terrigenous detritus can provide nutrients for marine organisms, promote the flourishing of lower aquatic organisms, and is also a key factor in the enrichment of OM. However, Froelich et al. (1979) believed that the input of terrigenous debris into the seabed as a diluent resulted in the loss of OM. In fact, OMA is comprehensively influenced by geological processes, including redox conditions, primary productivity, water restriction, and terrigenous detrital input (Peng et al., 2023; Zhang et al., 2023).

Recently, geochemical studies have been carried out on the WF-LMX shale. Current studies have suggested that the environmental contexts of the Late Ordovician and Early Silurian were different (Zou et al., 2019). The paleoenvironment is the material basis that controls petroleum generation and accumulation in marine shale systems. However, there are few studies on the differences and mechanisms of OMA in deep reservoirs between the WF and LMX shales. In the present study, fresh core collected from recent shale gas exploration wells in the Dingshan area are selected to systematically investigate the three parts, including the WF, long-1_1, and long-1_2 shale. The objectives of this study are summarized as follows: (a) To determine how various environmental factors are reconstructed, and the effects of paleoproductivity, redox conditions, terrigenous debris input, sedimentation rate, paleoclimate, and upwelling on OMA are studied in detail. (b) To identify the differences and mechanisms of OMA in two sets of high-quality shales, the WF and long-1_1 shales, are emphatically discussed. These results provided new perspectives on the exploration and development potential of deep shale gas in the Sichuan Basin.

2 Geological setting

The Sichuan Basin, which is situated in southwestern China, tectonically belongs to the Upper Yangtze Platform (Liu et al., 2021b). The Kwangsian movement caused compression on the Upper Yangtze Platform during the Late Ordovician and Early Silurian, resulting in the formation of a constrained shelf basin (Chen et al., 2004; Gao et al., 2022), and forming several uplifts in and around the Sichuan Basin, such as the central Sichuan, central Guizhou and Jiangnan uplifts (Lu et al., 2021). Additionally, two large-scale global transgressions occurred in the Late Ordovician and Early Silurian (Khan et al., 2019; Gao et al., 2022). Against this background, deep-water shelf sedimentation developed extensively in the Sichuan Basin, while the shallow shelf deposits at the edge of the uplift are dominated by organic-poor siltstones (Figure 1; Wang et al., 2020; Lu et al., 2021; Wang H. Y. et al., 2022).

The Dingshan area is in the southeastern Sichuan Basin. The region experienced tectonic uplift during the Caledonian and burial during the Hercynian-Indian movement, as well as folding and rupture during the Yanshan-Himalayan movement (Cao et al., 2021). The present-day tectonics of the Dingshan area consist of a series of steep backslopes and fracture zones trending NE and NNE that are trough folds (Huang et al., 2011).

In addition to the absence of Devonian, Carboniferous, and Cenozoic strata, other layers are relatively well-developed in the Dingshan area, with the WF-LMX Formation being the primary focus of this study. The WF-LMX Formation consists mainly of siliceous, silty, calcareous, and sandy shale (Lu et al., 2021; Zheng et al., 2024). The high-quality shale (TOC >2%) at the bottom of the WF-LMX Formation is notably characterized by thin layering, high TOC and silicon contents. In the Dingshan area, the WF-LMX Formation hosts high-quality shale reservoirs. The burial depth is approximately 4,000 m, the thickness of the OM-rich shale is approximately 80 m, while that of high-quality shale ranges from 28.9 to 35.5 m (Wei et al., 2020).
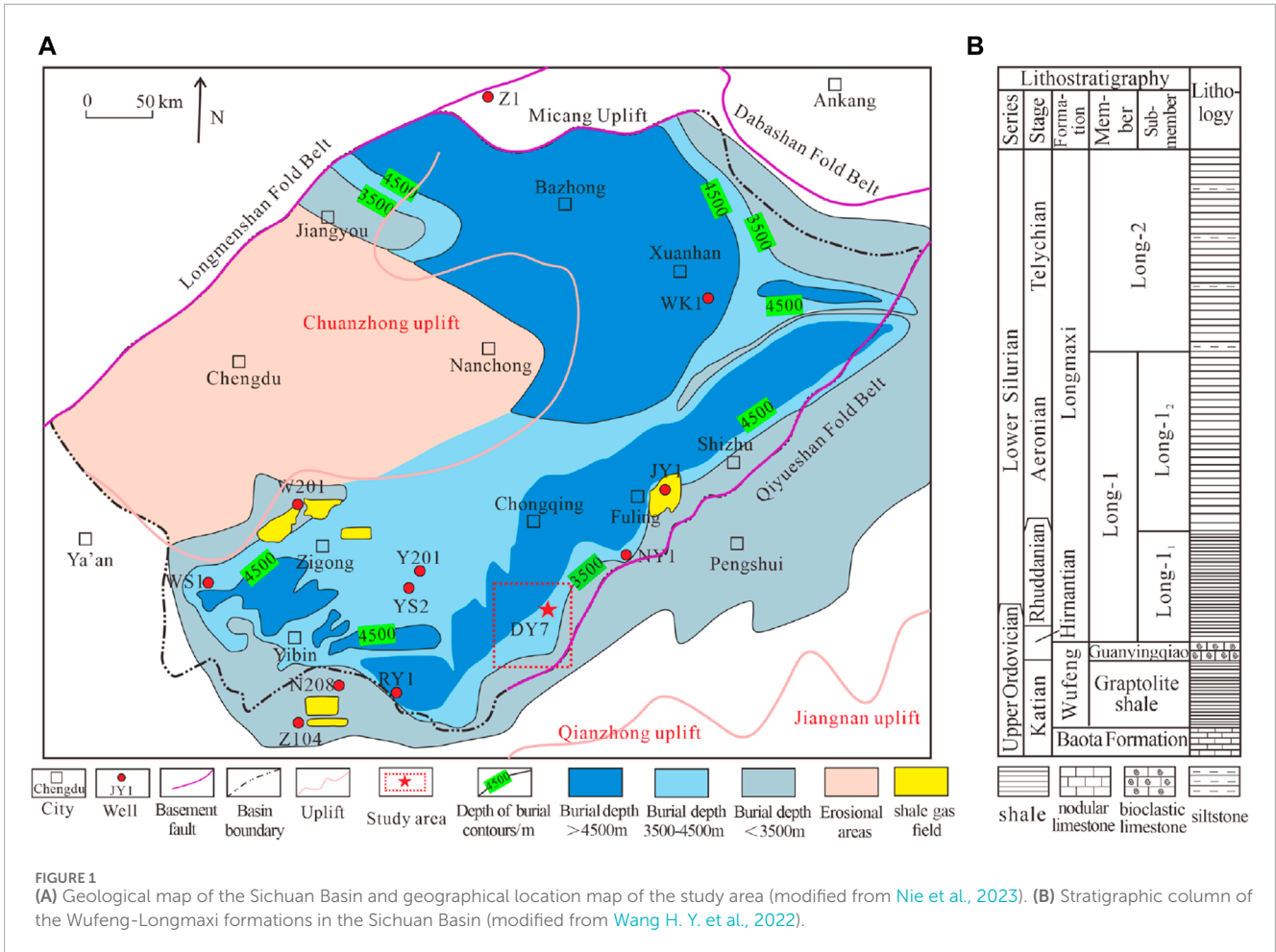
FIGURE 1
(A) Geological map of the Sichuan Basin and geographical location map of the study area (modified from Nie et al., 2023). **(B)** Stratigraphic column of the Wufeng-Longmaxi formations in the Sichuan Basin (modified from Wang H. Y. et al., 2022).
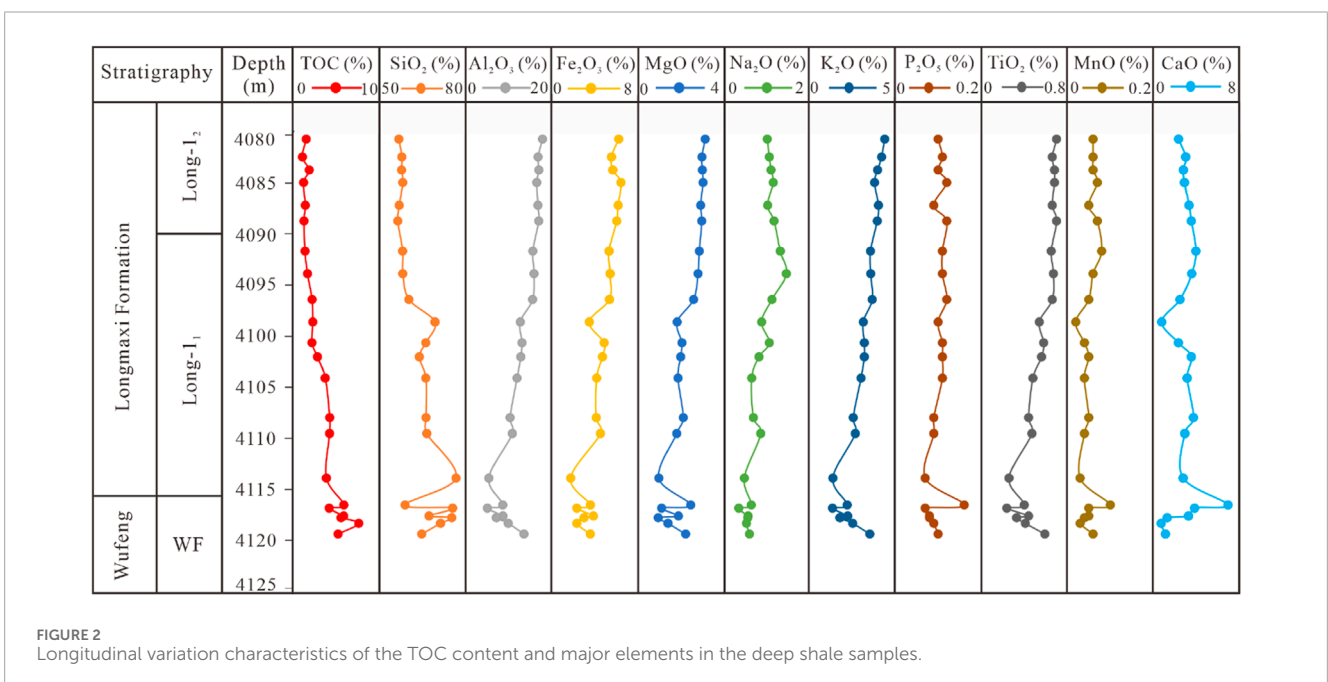
FIGURE 2
Longitudinal variation characteristics of the TOC content and major elements in the deep shale samples.
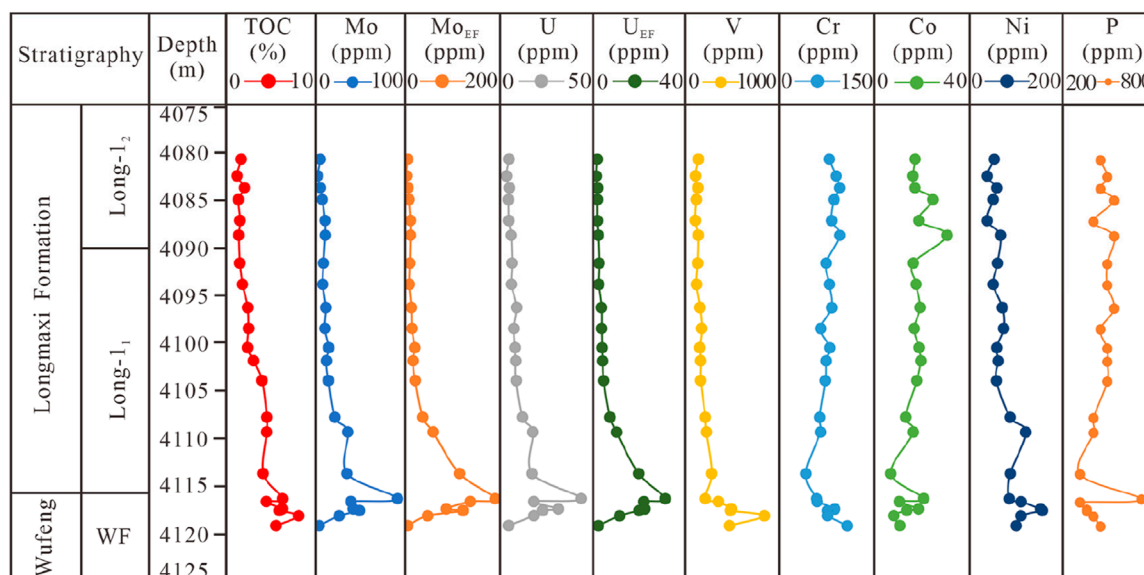
FIGURE 3
Characteristics of longitudinal variations in trace elements in deep shale samples.

3 Sample and methods

3.1 Sample

Fresh shale samples were taken from well DY7 in the Dingshan area, southeast Sichuan (Figure 1). The WF shale is mainly gray-black carbonaceous shale with a thickness of 2.84 m. The Long-1$_1$ shale is mainly gray-black (carbonaceous) shale with a thickness of 24.75 m. The Long-1$_2$ shale is mainly black-gray silty shale, with a thickness of 10.91 m. A total of 22 representative samples were selected, including six samples from Long-1$_2$, 10 samples from Long-1$_1$ and six samples from the WF (Supplementary Table S1).

3.2 Analysis

3.2.1 TOC test

The samples were crushed and sieved through a sieve of less than 200 mesh, 150 mg of each powdered sample was weighed and then removing carbonate minerals. The TOC contents were determined using a LECO CS230 analyzer.

3.2.2 Element testing

The major element tests were carried out by an X-ray fluorescence spectrometer (instrument model: AXios-mAX). The 200 mesh powdered samples were dried at 105°C for 2–3 h. First, 0.7 g of each sample and 7 g of Li$_2$B$_4$O$_7$ reagent were weighed and mixed, and then melted at 1,150°C to form a glass slice, which was then tested on an X-fluorescence spectrometer. An analytical precision was better than ±5% (Tan et al., 2021).

The trace and rare earth elements contents of the samples were testing by was an ICP-MS (instrument model: ICAP RQ). An analytical precision was better than ±10%. The detailed analysis is described in the references (Yang, et al., 2021; He et al., 2022).

3.3 Proxy calculations

The enrichment factors (EF) can be used to evaluate the enrichment degree of trace elements in shales (Algeo and Tribovillard, 2009). The calculation formula of EF (Wedepohl, 1971) is as Equation 1:

$$X_{EF} = \frac{(X/Al)_{\text{sample}}}{(X/Al)_{\text{PAAS}}} \tag{1}$$

where, X is the trace element content of the shale sample, and PAAS is a standard shale reference based on the Post-Archean Australian Shale (Taylor and McLennan, 1985). $X_{EF} > 1$ indicates that the shale sample is more enriched in element X relative to the PAAS.

Anoxic conditions are more favorable for the preservation of OM but not for the preservation of P, as the reductive dissolution of ferric hydroxide could result in the release of P from sediments. P will be adsorbed on the surface of iron hydroxide to be preserved in sediments under both oxic and anoxic conditions, corresponding to the deficiency or enrichment of organic carbon (Algeo and Ingall, 2007; Steenbergh et al., 2011). Therefore, the mole ratio of Corg/P can be used to characterize the redox conditions, and its calculation formula is as Equation 2:

$$Corg = \frac{\frac{TOC}{12}}{\frac{P}{30.97}} \tag{2}$$

The chemical index of alteration (CIA) is a reliable indicator for assessing chemical weathering intensity (McLennan et al., 1993; Lu et al., 2024), reflecting the paleoclimate evolution of the sedimentary source area, and the CIA is calculated as Equation 3 (Nesbitt and Young, 1982; Lu et al., 2024).

$$CIA = \frac{Al_2O_3}{Al_2O_3 + CaO^* + Na_2O + K_2O} \times 100\% \tag{3}$$
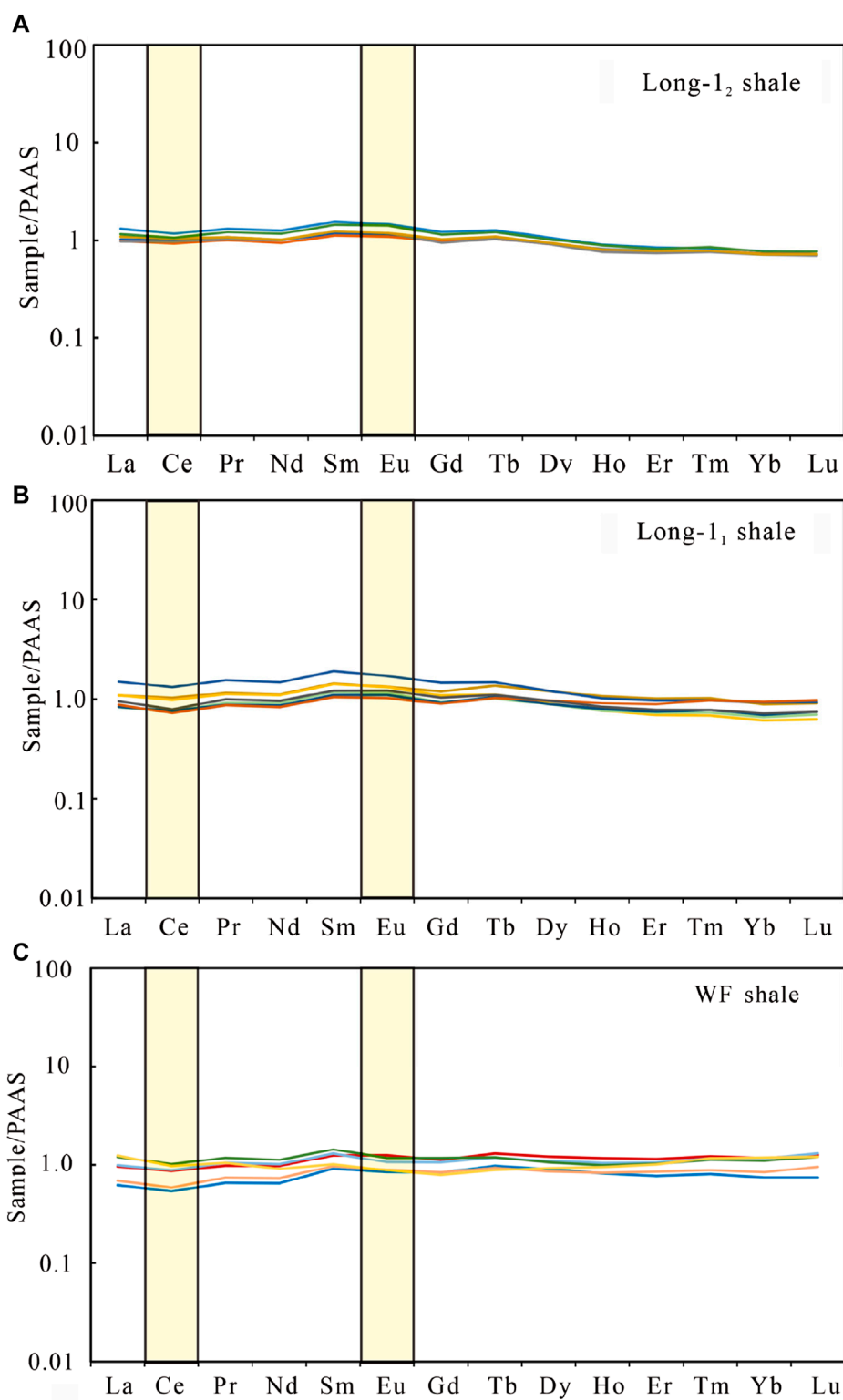
FIGURE 4
PAAS normalized REE distribution model of the **(A)** Long-1_2, **(B)** Long-1_1, **(C)** WF shale samples.
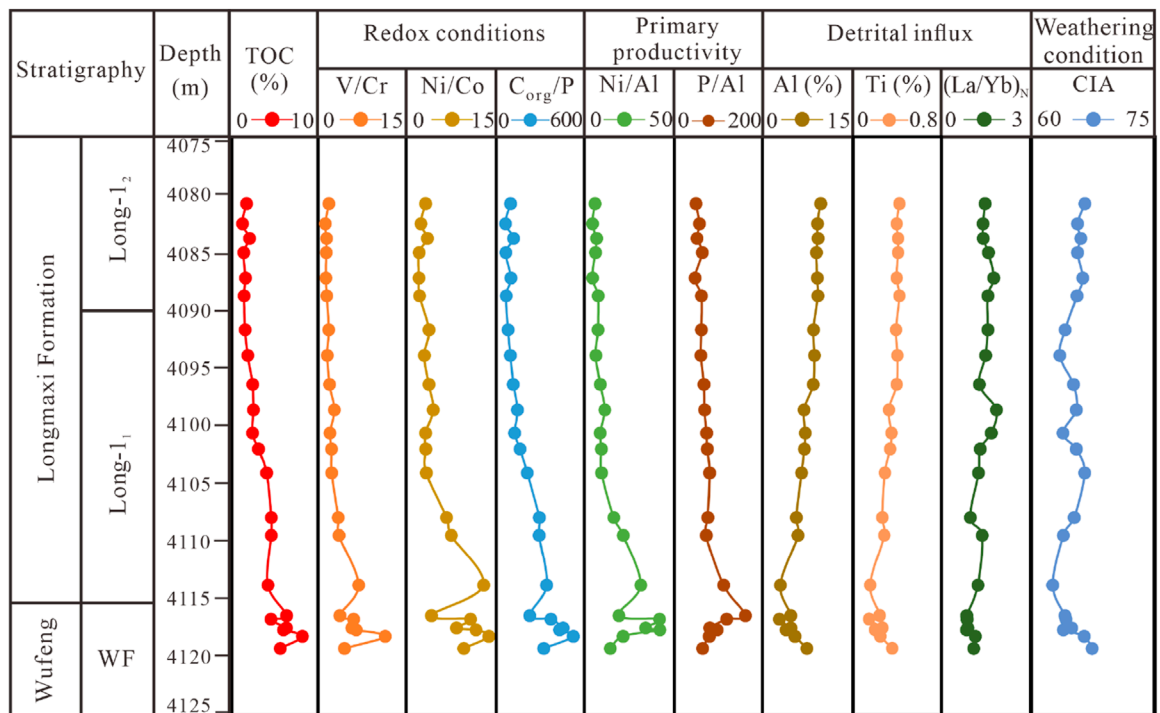
FIGURE 5
Longitudinal variation characteristics of geochemical indexes of deep shale samples.
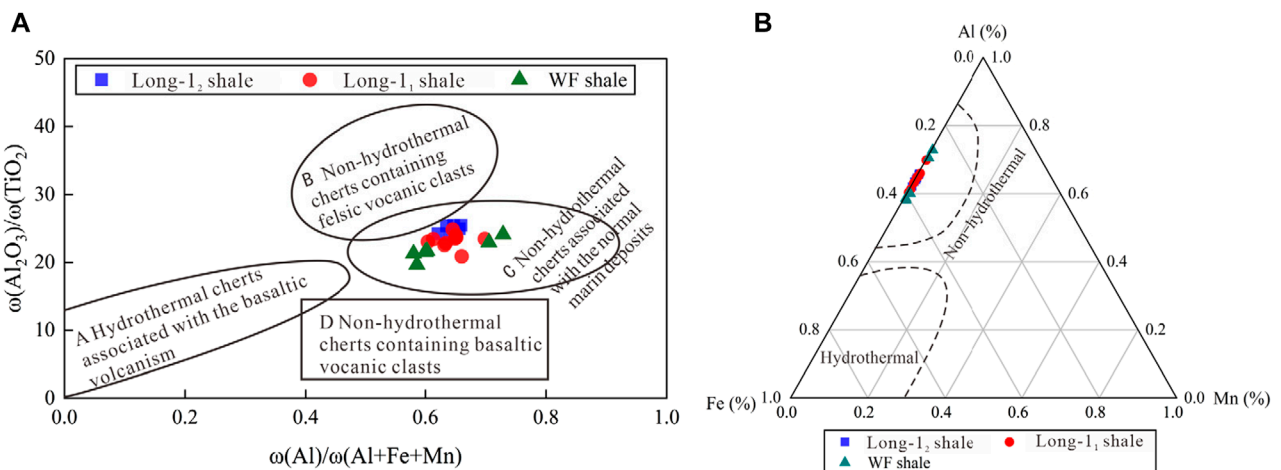
FIGURE 6
(A) Al_2O_3/TiO_2 vs. (Al)/(Mn+Al+Fe) (Feng et al., 2023a); **(B)** Al-Fe-Mn ternary diagram (Adachi et al., 1986).

The chemical formula for oxides is in moles, CaO^* refers to CaO in silicate minerals, and non-silicate minerals should be removed in the calculation, the formula for CaO^* is as Equations 4, 5 (McLennan et al., 1993):

$$CaO_{(adjusted)} = CaO - \left(\frac{10}{3} \times P_2O_5\right) \quad (4)$$

$$CaO^* = \begin{cases} Na_2O, CaO_{(adjusted)} > Na_2O \\ CaO_{(adjusted)}, CaO_{(adjusted)} \leq Na_2O \end{cases} \quad (5)$$

4 Results

4.1 Organic matter amount

The TOC contents of the studied shale samples are shown in Supplementary Table S1. In general, the TOC contents show a gradually decreasing trend from bottom to top, but the variations in the different layers differed (Figure 2). The TOC contents of the WF shale are higher, ranging from 4.20% to 7.62% (mean: 5.73%), which

FIGURE 7
Ti-Al diagram of the deep shale samples.
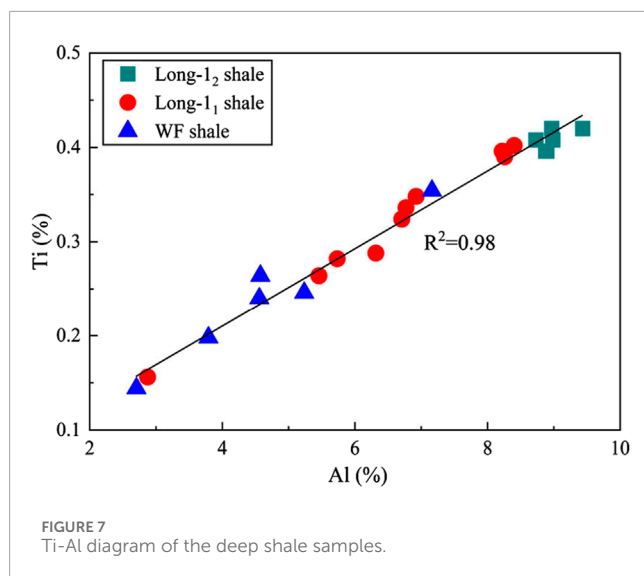
shows significant longitudinal fluctuations. The TOC contents of the Long-1$_1$ shale are high, ranging from 1.42% to 4.26% (mean: 2.89%), and show an obvious gradually decreasing trend. The TOC contents of the Long-1$_2$ shale are low, ranging from 1.13% to 1.91% (mean: 1.44%). Vertically, the values consistently remain at a low level with no pronounced patterns of variation discernible.

4.2 Major elements

In this study, the major elements of the WF-LMX shale mainly consist of SiO_2, Al_2O_3 and Fe_2O_3. The SiO_2 contents range from 56.45% to 76.65% (64.05% on average). The Al_2O_3 contents range from 5.11% to 17.82% (12.67% on average). The Fe_2O_3 contents range from 1.77% to 6.41% (4.48% on average). The MgO, Na_2O, K_2O and CaO contents in the shale are 0.93%–3.10%, 0.36%–1.46%, 1.37%–4.38%, and 0.78%–6.96%, respectively. The shale contains small amounts of P_2O_5, TiO_2 and MnO, the contents of which are 0.07%–0.16%, 0.24%–0.70% and 0.02%–0.10% respectively (the specific data are shown in Supplementary Table S1).

The major element contents are significantly different in the WF, Long-1$_1$ and Long-1$_2$ shales (Figure 2). The SiO_2 contents in the WF (59.01%–75.45%, average of 68.84%) and Long-1$_1$ (58.15%–76.65%, average of 65.20%) shales are higher than that of the Long-1$_2$ shale (56.45%–58.19%, average of 57.35%). On the contrary, the Al_2O_3 and Fe_2O_3 contents of Long-1$_2$ are higher than those of in the WF and Long-1$_1$ shales. For these three shales, the average Al_2O_3 contents are 8.82%, 12.40%, and 16.97%, respectively, and the average Fe_2O_3 contents are 3.12%, 4.38%, and 6.00%, respectively. The MgO, K_2O and TiO_2 contents in the WF and Long-1$_1$ shales are lower than those in the Long-1$_2$ shale, while the Na_2O contents in the Long-1$_1$ shale are the highest.

4.3 Trace elements

As shown in Figure 3, compared with the long-1$_2$ shale, the Mo, U, V and Ni concentrations in the WF and Long-1$_1$ shales are more

obviously enriched. Vertically, these elements increase first and then decrease from the bottom to the top. However, Cr, Co and P fluctuate but have no obvious trend (see Supplementary Table S2). Compared with the PAAS (Wedepohl, 1971), the Mo and U contents of these shales in the present study are relatively enriched. The Mo_{EF} of the WF, Long-1$_1$ and Long-1$_2$ shales are 4.96–188.86 (average of 97.39), 8.70–114.00 (average of 31.19) and 2.25–11.16 (average of 7.12), respectively. The U_{EF} of these three shales are 2.11–30.25 (average of 17.60), 2.37–19.08 (average of 5.98), and 1.26–2.14 (average of 1.72), respectively.
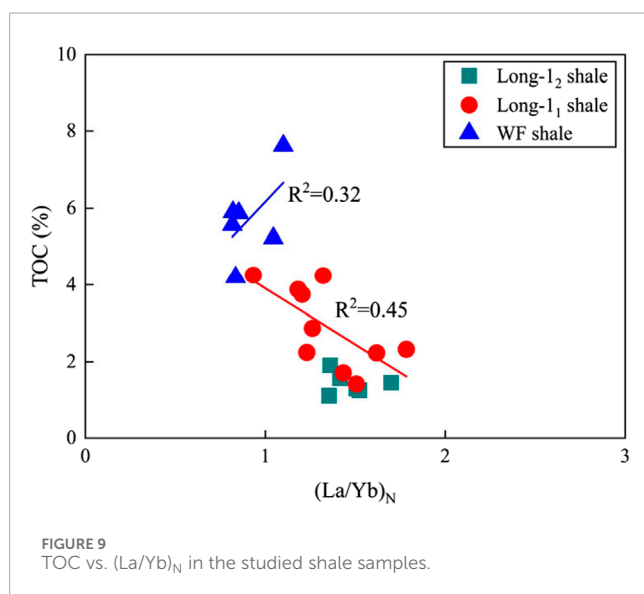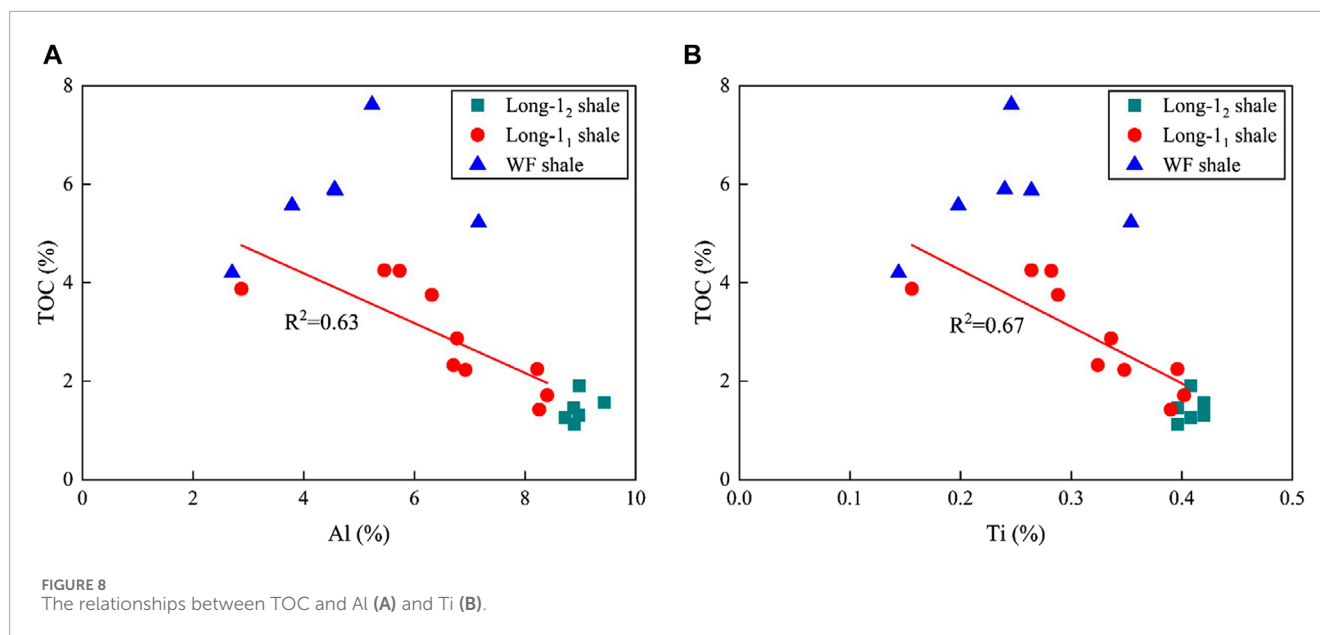
4.4 Rare earth elements

The rare earth element contents of the studied samples are shown in Supplementary Table S3. The contents of rare earth elements (ΣREE) in the WF, Long-1$_1$, and Long-1$_2$ shales range from 115.06 to 203.78 ppm (mean: 164.73 ppm), 93.14–277.37 ppm (mean: 186.44 ppm), and 174.70–225.97 ppm (mean: 194.18 ppm), respectively. From bottom to top, ΣREE is increasingly abundant. The ΣREE of all three shales are higher than the average value of the upper continental crust (146.4 ppm; McLennan, 2001), and the ΣREE of the WF and Long-1$_1$ shales are less than the North American shale (193.18 ppm; Gromet et al., 1984). The REE content of the WF shale is lower than that of the PAAS, while the ΣREE of the Long-1$_1$ and Long-1$_2$ shales is slightly higher than that of the PAAS (184.77 ppm; Taylor and McLennan, 1985).

For the WF, Long-1$_1$, and Long-1$_2$ shales, the average contents of light rare earth elements (LREE) are 147.10 ppm, 169.39 ppm, and 178.10 ppm, respectively. Moreover, the average contents of heavy rare earth elements (HREE) are 17.63 ppm, 17.05 ppm, and 16.08 ppm, respectively, and the LREE/HREE ratios are 8.30, 9.82, and 11.06, respectively, which are higher than those of North American shale (7.83; Larry et al., 1966), indicating a relative enrichment of LREE and deficit of HREE in the studied shale. The average $(La/Yb)_N$ (normalized by the PAAS) values of the WF, Long-1$_1$ and Long-1$_2$ shales are 0.91, 1.35 and 1.48, respectively (Figure 4).

5 Discussion

5.1 Paleoclimatic conditions

The degree of chemical weathering of source rocks is controlled by temperature and humidity. Generally, a cold and dry environment is not conducive to chemical weathering, while a warm and humid environment is conducive to chemical weathering (Nesbitt and Young, 1982). The CIA is used to reflect the intensity of chemical weathering. CIA values of 50–65, 65–85, and 85–100 reflect cold and dry climate conditions, warm and humid climate conditions, and hot humid subtropical-tropical climates, respectively, with increasing weathering intensity (Nesbitt and Young, 1989; Nesbitt and Young, 1996). For the WF shale, as shown in Figure 5, the CIA values decrease with decreasing burial depth, reflecting a gradually colder climate corresponding to a widespread global ice age. Subsequently, for the Long-1 shale, although there are some fluctuations, the CIA increased gradually overall, reflecting the change in paleoclimate toward warm and humid conditions, accompanied by an increase in weathering intensity.

FIGURE 8
The relationships between TOC and Al **(A)** and Ti **(B)**.

FIGURE 9
TOC vs. (La/Yb)$_N$ in the studied shale samples.

5.2 Detrital influx and sedimentation rate

Mn, Al and Fe are commonly used to determine the silicon source. Al is generally the representative element of terrigenous detrital input, and Mn and Fe are generally related to submarine hydrothermal activity, therefore, the $\omega(Al)/\omega(Mn+Al+Fe)$ ratio can be used to identify the origin of silicon (Adachi et al., 1986). In addition, researchers often use $\omega(Al_2O_3)/\omega(TiO_2)$-$\omega(Al)/\omega(Mn+Al+Fe)$ to distinguish silicon sources (Feng et al., 2023a). According to Figures 6A, B, the $\omega(Al)/\omega(Mn+Al+Fe)$ values of the WF, Long-1$_1$ and Long-1$_2$ shales are 0.58–0.73, 0.60–0.70 and 0.62–0.66, respectively, with average values of 0.63, 0.64 and 0.64, indicating that their silicon sources should be the non-hydrothermal source (Gao et al., 2022). Fe$_2$O$_3$ and MnO are

1.77%–6.41% (mean: 4.48%) and 0.02%–0.10% (mean: 0.05%), respectively, suggesting that these three shales are of normal marine non-hydrothermal origin.

Al and Ti are the main components of the continental crust, Al mainly exists stably in the form of aluminosilicate minerals (Calvert and Pedersen, 1993), and Ti mainly exists in the form of heavy minerals (e.g., ilmenite) (Tribovillard et al., 2006). Al and Ti are stable during diagenesis and are less affected by diagenesis, so they are often used to indicate terrigenous detrital input. The lower the contents of Al and Ti are, the less affected they are by terrigenous input (Walker et al., 1988). Previous studies have shown that Al and Ti are strongly positively linearly correlated (Jin et al., 2020b), and Al can be used as an index of terrigenous detrital input. In this study, there is a strong positive linear correlation between Al and Ti ($R^2 = 0.98$) in the shale samples. (Figure 7). The input of terrigenous debris has many effects on the enrichment and preservation of OM (Froelich et al., 1979), because changes in terrigenous detrital input may affect the concentration of OM in marine sediments.

In the WF, Long-1$_1$ and Long-1$_2$ shales, the content of Al shows a trend of decreasing first and then increasing (Figure 5). Their Al contents are 2.71%–7.16% (average of 4.67%), 2.87%–8.40% (average of 6.57%) and 8.73%–9.43% (average of 8.98%), respectively. Consistent with the variation in Al, the corresponding Ti contents are 0.14%–0.35% (mean: 0.24%), 0.16%–0.40% (mean: 0.32%) and 0.40%–0.42% (mean: 0.41%), respectively. For the deep shales in this study, the increase in terrigenous input flux gradually increasing upward. Furthermore, the trend of variation of the terrigenous detrital input is opposite to that of TOC, confirming the negative synergistic relationship between TOC and terrestrial input indicators. (Figures 8A, B).

The difference in burial rate will affect the preservation of OM, thereby affecting its enrichment (Canfield, 1994). (La/Yb)$_N$ can reflect the sedimentation rate, and this proxy is positively correlated with the sedimentation rate (Zeng et al., 2015; Zheng et al., 2022). Our study found that the (La/Yb)$_N$ values of the WF, Long-1$_1$ and
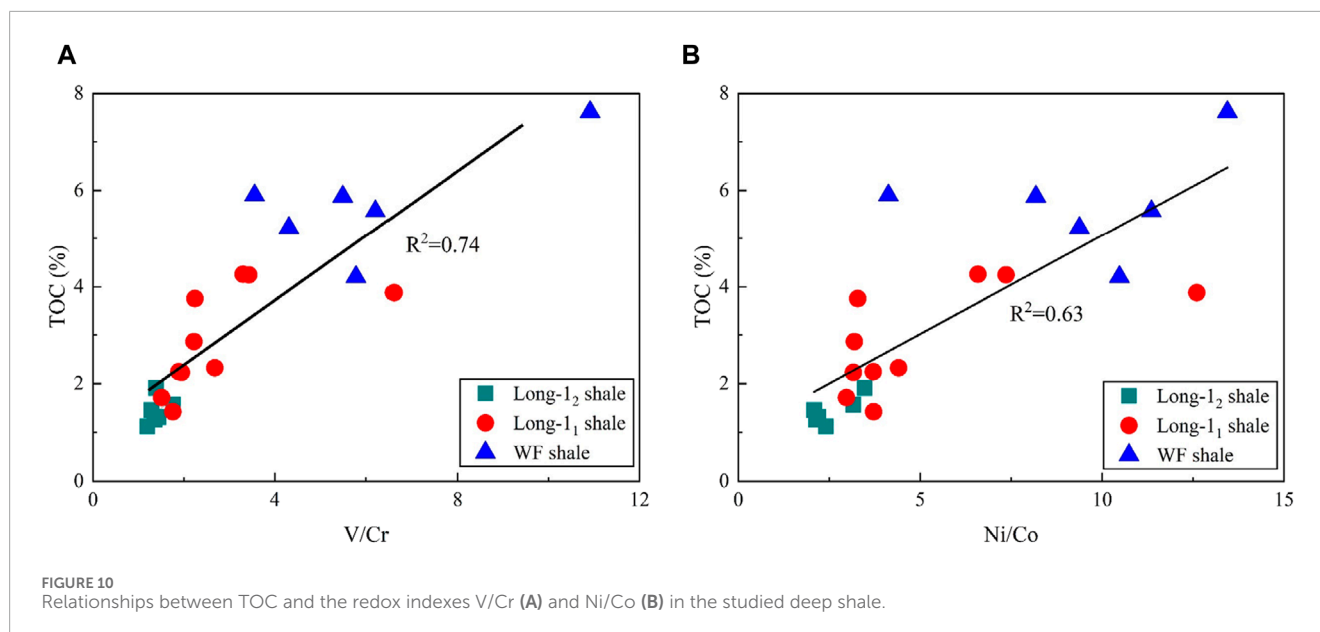
FIGURE 10
Relationships between TOC and the redox indexes V/Cr **(A)** and Ni/Co **(B)** in the studied deep shale.
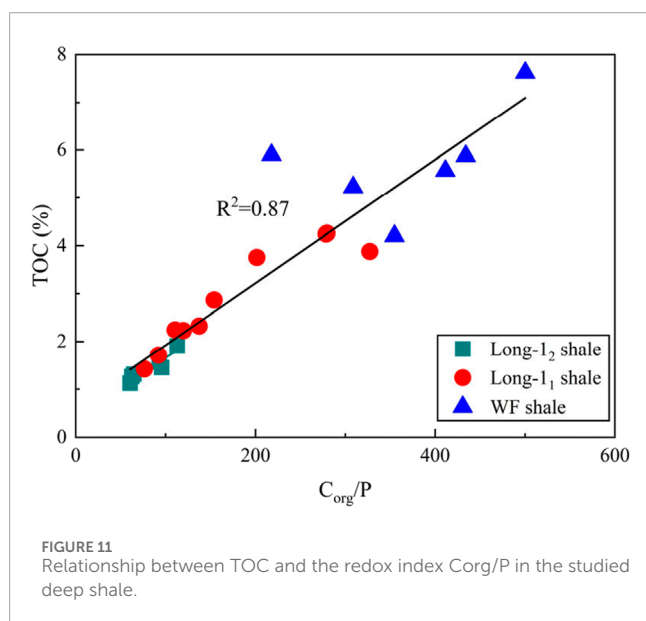

FIGURE 11
Relationship between TOC and the redox index Corg/P in the studied deep shale.

Long-1_2 shales range from 0.82 to 1.10 (mean: 0.91), 0.93–1.78 (mean: 1.36) and 1.35–1.70 (mean: 1.47), respectively. In terms of the sedimentation rate, the sedimentation rate gradually increases from bottom to top. As shown in Figure 5, an increase in the sedimentation rate would lead to a decrease in the OM content in the studied shales. However, the sedimentation rate appears to have a different effect on the various shale layers (Figure 9). The lower sedimentation rate contributes to the OMA in the WF shale. For the WF shale, an increase in the sedimentation rate helps to reduce the probability of OM being destroyed by oxidation during the sedimentation process. For the Long-1 shale, its sedimentation rate is obviously higher than that of the WF shale. Especially for the organic-rich shale of Long-1_1, the increase in sedimentation rate is synchronous with the decrease in TOC content.

5.3 Redox and water restriction conditions

The redox conditions of the water column are one of the contributing factors to OMA, to which, an anoxic, oxygen-deficient environment is particularly conducive (Algeo and Maynard, 2004). Redox-sensitive elements such as Mo, U, V, Cr, Co, Ni and Th have been widely used to assess the redox conditions of marine water bodies (Algeo and Lyons, 2006).

Although these redox-sensitive elements can be used to judge paleoredox conditions, an individual element is easily affected by factors such as the geological environment (Jones and Manning, 1994). Therefore, the trace element ratio is introduced to reconstruct the redox conditions of bottom water. Paleoredox indicators such as V/Cr and Ni/Co can serve as indicators to evaluate the paleoredox environment. The V/Cr ratio indicates the boundaries of oxic, dysoxic and anoxic environments at 2.00 and 4.25, respectively. For Ni/Co, the larger the ratio is, the more reductive the bottom water environment, with limits for oxic, dysoxic and anoxic environments at 5.00 and 7.00, respectively. In the WF shale, the V/Cr ratio ranges from 3.55 to 10.91 (6.04 on average), and the Ni/Co ratio ranges from 4.13 to 13.44 (9.49 on average). Similarly, in the Long-1_1 shale, the V/Cr ratio ranges from 1.51 to 6.61 (2.76 on average), and the Ni/Co ratio ranges from 2.97 to 12.60 (5.10 on average). Finally, in the Long-1_2 shale, these two proxies are 1.19–1.76 (1.40 on average) and 2.08–3.47 (2.57 on average), respectively. The variation trend in the profile of this study is consistent, depicting a transformation from strongly reducing conditions to an oxygen-deficient, dysoxic-oxic environment. Furthermore, there is a positive relationship between TOC and the redox proxy (Figure 5; Figure 10).

Previous studies have indicated that the Corg/P ratio indicates the boundaries of oxic, dysoxic and anoxic environments at 50 and 100, respectively. (Algeo et al., 2020). The Corg/P values range between 217.91 and 500.30 (mean: 371.21) for the WF shale, between 76.48 and 327.36 (mean: 177.78) for the Long-1_1 shale, and between 60.53 and 112.87 (mean: 81.48) for the Long-1_2 shale. These data further confirm that the three sets of shales formed under
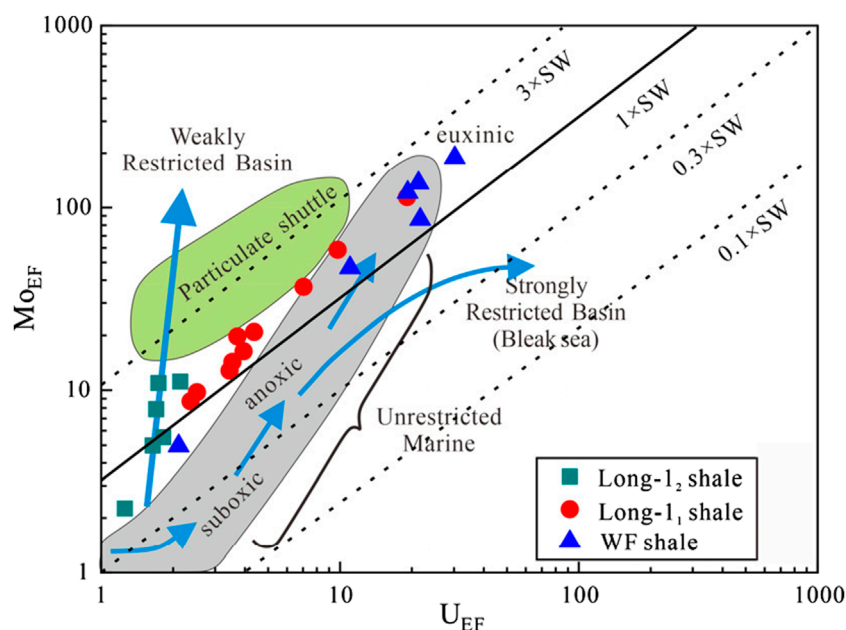
FIGURE 12
Mo$_{EF}$ versus U$_{EF}$ in the studied deep shale samples (modified from Algeo and Tribovillard, 2009).
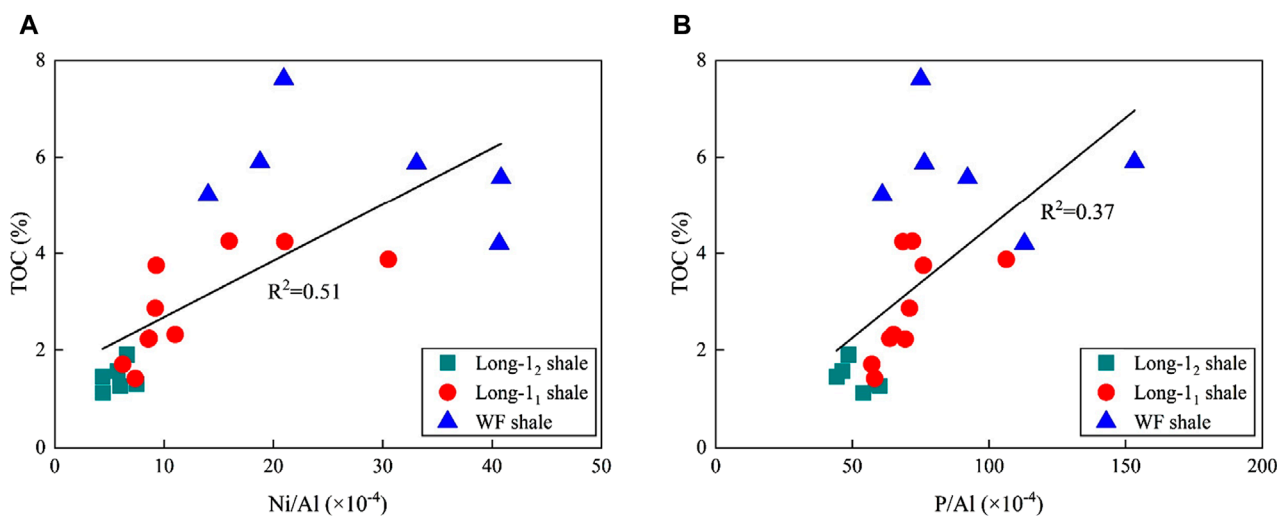
FIGURE 13
Relationships between TOC and Ni/Al (A) and P/Al (B) in the studied deep shale.

different redox conditions as suggested by the redox agent discussed previously, i.e., from bottom to top, the transition from anoxic to dysoxic-oxic conditions (Figure 5). The Corg/P values of the Long-1$_1$ and WF shales are significantly higher than those of Long-1$_2$, indicating that deposition under more anoxic conditions is more conducive to OMA (Figure 11).

The Mo$_{EF}$ and U$_{EF}$ excluding terrigenous debris can be used as indicators of water restriction and redox conditions. In the WF shale, the Mo$_{EF}$ values range from 4.96 to 188.86 ppm, while the U$_{EF}$ values range from 2.11 to 30.25 ppm. In the Long-1$_1$ shale, the ranges are 8.70–114 ppm and 2.37–19.08 ppm, respectively. In

the Long-1$_2$ shale, the ranges are 2.25–11.16 ppm for the Mo$_{EF}$ and 1.26–2.14 ppm for the U$_{EF}$. The enrichment rate of Mo is higher than that of U in the shale, and thus the Mo/U (Mo$_{EF}$/U$_{EF}$) ratio tends to increase. The Mo$_{EF}$/U$_{EF}$ distribution in the Long-1$_1$ shale and the WF shale ranges from 1 to 3×SW, while in the Long-1$_2$ shale, it is nearly 1×SW. This means a transition in the covariant modes of Mo$_{EF}$ and U$_{EF}$ from 3×SW to 1×SW and 0.3×SW from bottom to top, suggesting a shift from relatively sufficient to insufficient Mo supply. This shift reflects a change in the sedimentary water body from an open environment to a restricted environment and a transition from reduction to oxidation (Figure 12).

FIGURE 14
Zr/Cr versus Zr/Al_2O_3 in the studied deep shale, Zr/Cr = 1.0 ppm/ppm, Zr/Al_2O_3 threshold = 6.0 ppm/wt% (threshold value cited Yang et al., 2022).
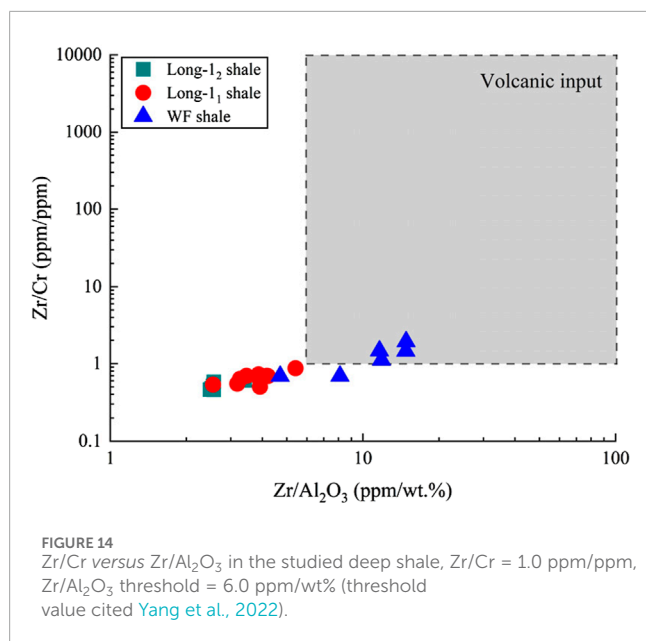
To sum up, the redox indexes in the WF-LMX shale exhibit a consistent change trend in this study. The bottom water of the WF shale is predominantly characterized by an oxygen-deficient vulcanization environment. During the deposition period of the Long-1 shale, the reduction weakens gradually from the bottom to the top, with the Long-1_1 shale being dominated by an anoxic environment, and the Long-1_2 shale exhibiting an oxidizing environment. Under anoxic conditions, the OM in shale is more likely to be preserved (Figures 10, 11).

5.4 Paleoproduction

In geological history, paleoproductivity has been a crucial measure of the OM produced by ancient marine organisms per unit area and per unit time. It significantly influences the accumulation of OM in geological records (Luo et al., 2013). Trace elements serve as effective indicators for reconstructing primary productivity (Tribovillard et al., 2006). P is not only one of the important nutrient elements in biological metabolism, but also a component of the skeleton of marine organisms, and precipitates with sediments after death. Ni plays a vital role in photosynthesis in marine phytoplankton, and the higher the Ni content is, the higher the organic mass in the sediment (Vink et al., 1997; Piper et al., 2004). After excluding the influence of terrigenous clasts, P/Al and Ni/Al can be used to evaluate the level of primary productivity. Larger values of these proxies indicate higher levels of paleoproductivity (Tribovillard et al., 2006; Pan et al., 2020).

The current investigation reveals that the P/Al ($\times 10^{-4}$) ratio ranges from 60.96 to 153.26 (mean: 95.13), and the Ni/Al ($\times 10^{-4}$) ratio varies from 14.03 to 40.83 (mean: 28.06). Specifically, the P/Al ($\times 10^{-4}$) for the Long-1_1 shale ranges from 57.16 to 106.32 (average of 70.73), while the Ni/Al ($\times 10^{-4}$) varies from 6.22 to 30.51 (average of 12.78). Meanwhile, the Long-1_2 shale exhibits a P/Al ($\times 10^{-4}$) range of 44.26–60.02 (average of 51.93) and

a Ni/Al ($\times 10^{-4}$) range of 4.38–7.48 (average of 5.77). Notably, the trends in the P/Al and Ni/Al ratios show similar patterns (Figure 5). Subsequently, the primary productivity levels during the sedimentary period of the WF shale increased with decreasing depth. In contrast, the overall productivity in the Long-1 shale gradually decreases from bottom to top. Moreover, the TOC content of the Long-1_1 shale demonstrates a linear relationship with productivity, whereas the primary productivity of the WF and Long-1_2 shales displays a weaker relationship with TOC (Figure 13). This suggests that the productivity of the Long-1_1 shale positively influences its OMA.

Numerous studies have shown that there is a close relationship between volcanic eruptions and marine life. For example, the eruption of the Anatahan volcano in 2003 increased the level of productivity in the nutrient-poor region of the Pacific Northwest. The 2008 eruption of the Kasatochi volcano in the United States also promoted the reproduction of marine life (Qiu et al., 2019). During the formation of the WF shale, an area with frequent volcanic activity in the Upper Yangtze region (Li et al., 2017; Qiu et al., 2019), Yang et al. (2022) used the intersection diagram of Zr/Cr and Zr/Al_2O_3 to identify the presence of volcanic ash. In the present study, the nutrient flux and accompanying increased productivity of the WF shale originated from the input of volcanic ash (Figure 14). Previous studies have shown that intense volcanic activity has a dual-promoting effect on the OMA in shale (Wu et al., 2018). On the one hand, frequent volcanic eruptions led to the release of significant amounts of volcanic ash, which contributed to the rapid growth of marine surface producers and provided ample food sources for symbiotic siliceous organisms and algae, thereby increasing marine organism productivity (Figure 5). On the other hand, intense volcanic activity resulted in the formation of an extremely anoxic environment and the deterioration of seawater properties. Consequently, some organisms were unable to adapt and died over a wide area, with their remains rapidly deposited and buried before oxidative decomposition, thereby preserving OM.

5.5 Implications for organic matter accumulation

The formation of organic-rich shales in marine environments is a complex process influenced by many factors. Globally, it is generally related to the activity cycle of ice age and plate movement (Shen et al., 2023). At the basin level, factors such as primary productivity, redox conditions, terrigenous detrital input and sedimentation rate play significant roles in controlling OMA (Demaison and Moore, 1980; Wu et al., 2021). The primary factors controlling OMA can vary distinctly across different stages, particularly during the complex geological events of the Late Ordovician and Early Silurian periods. Therefore, it is necessary to clarify the mechanism of OMA by considering the interplay between the main controlling factors and geological events.

By comparing the paleoclimate conditions during shale formation with the longitudinal variation trend of the TOC content (Figure 5), it is found that the chemical weathering index has no significant effect on the OMA. This can be attributed to
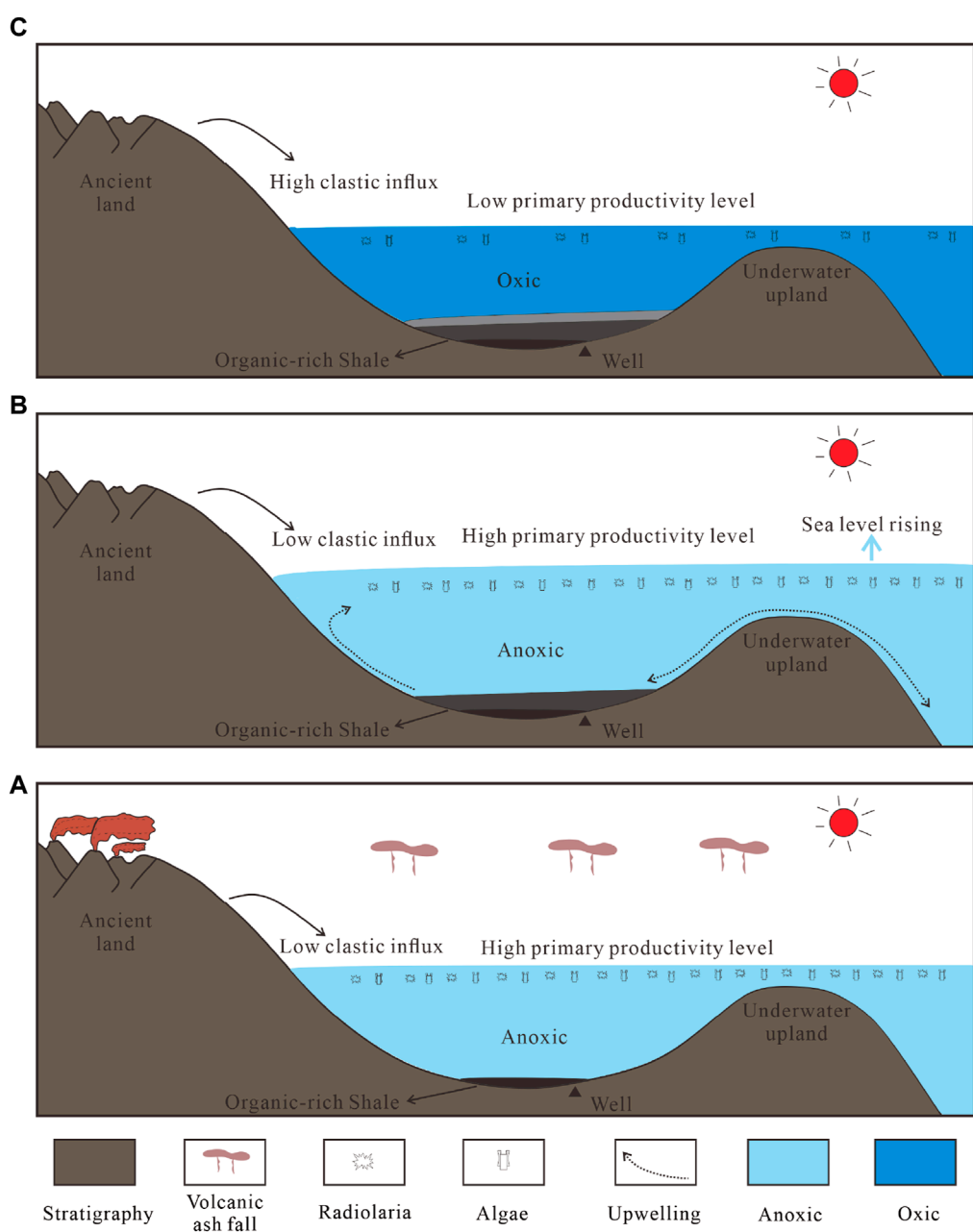
FIGURE 15
Organic matter enrichment model of the WF-LMX formation in the Dingshan area, Sichuan Basin. **(A)** WF shale; **(B)** Long-1_1 shale; **(C)** Long-1_2 shale.

the overall low to medium degree of chemical weathering during the sedimentation of the WF-Long-1 shales, indicating that individual climate factors had little influence on the OMA. These findings suggest that paleoclimate conditions are not the main controlling factor affecting the OMA.

Based on the aforementioned discussion, the OMA model of the WF-LMX Formation was established (Figure 15). In the early sedimentary stage of WF formation, tectonic uplift in the surrounding area led to the development of a barrier sea basin in the middle and upper Yangtze region. This basin experienced strengthened internal limitations, thereby creating a favorable environment for water retention (Li et al., 2017).

The occurrence of volcanic eruptions resulted in the injection of significant amounts of volcanic ash into the ocean. The dissolution of volcanic ash served to supplies abundant nutrients to marine water, thereby facilitating the proliferation of plankton. Furthermore, volcanic activity led to the creation of an anoxic environment. In addition, the temperature gradually decreased during the Late Ordovician sedimentation period, which would have strengthened the thermohaline circulation and thus contributed to the productivity improvement. The various paleoproductivity proxy indicators all confirmed the high productivity level during this period (Figure 5). The slow deposition rate mitigated the adverse influence of terrigenous debris input on OMA to a certain extent,

and finally resulted in the deposition of high-quality shale with a small thickness.

During the sedimentary period of the Long-1_1 shale (Figure 15B), the TOC content of the Long-1_1 shale is positively correlated with the redox environment and paleoproductivity to a certain extent (Figures 10, 11, 13) but negatively correlated with terrigenous clastic input and sedimentation rate indicators (Figures 8, 9). This restricts the OMA in the Long-1_1 shale to some extent. The results show that the OMA is mainly controlled by the synergistic positive effects of the redox environment and paleoproductivity. In addition, during the early Silurian period, there was a significant shift in climate from cold to warm conditions. This change was accompanied by global sea level rise, increasing temperatures, and the melting of glaciers. As a result, the Yangtze Sea was able to connect with the broad sea, leading to the development of upwelling (Jin et al., 2020a; Feng et al., 2023a), the upwelling brought nutrients to the surface, creating ideal conditions for the growth and proliferation of aquatic organisms. Moreover, global sea level rise exceeds tectonic uplift, resulting in a low degree of basin limitation. This, in combination with the input of terrigenous clastic material and increased sedimentation rates, partially hindered the further OMA. As a result, the TOC content of the Long-1_1 shale was found to be lower than that of the WF shale. Nonetheless, the Long-1_1 shale remains a high-quality shale overall.

During the sedimentary period of the Long-1_2 shale (Figure 15C). In the absence of nutrients provided by upwelling, nutrient-poor seawater resulted in a low level of primary productivity. Meanwhile, the terrigenous debris input and sedimentation rate increased and diluted the OM flux due to the decrease in sea level (Figure 5). These three factors, namely, OM deficit, low productivity level and poor bottom water preservation conditions are the fundamental reasons for the formation of organic-poor shale.

6 Conclusion

The depositional environments of the WF-LMX shale at well DY7 in the Dingshan area of the Sichuan Basin, were investigated, and the mechanisms driving the OMA were explored. This work culminates in several pivotal conclusions:

During the WF sedimentation period, a prevailing strongly reducing environment, coupled with frequent volcanic activities that supplied abundant nutrients, fostered conditions conducive to heightened productivity. Low terrigenous clastic input and sedimentation rates further promoted optimal preservation conditions. Consequently, the WF shale is characterized by a notably high TOC.

During the Long-1_1 sedimentation period, the organic-rich shale was positively influenced by a strong reducing environment and high paleoproductivity, while terrigenous clastic input and sedimentation rate somewhat restricted OMA. Therefore, the TOC content of the Long-1_1 shale is lower than that of the WF shale, yet it remains a high-quality shale.

During the Long-1_2 sedimentation period, the oxic conditions of the water column prevented the effective preservation of OM. Additionally, the increase in terrigenous clasts and sedimentation

rates further diluted the OM, leading to low productivity levels and subsequently low OM contents.

Data availability statement

The original contributions presented in the study are included in the article/Supplementary Material, further inquiries can be directed to the corresponding author.

Author contributions

QW: Conceptualization, Data curation, Methodology, Writing–original draft, Writing–review and editing. YF: Investigation, Supervision, Writing–review and editing, Writing–original draft. PG: Writing–review and editing. GM: Visualization, Writing–review and editing. CL: Investigation, Visualization, Writing–review and editing. QF: Formal Analysis, Methodology, Writing–review and editing. GL: Formal Analysis, Writing–review and editing. YT: Formal Analysis, Writing–review and editing. XX: Funding acquisition, Resources, Writing–review and editing.

Funding

Conflict of interest

The authors declare that the research was conducted in the absence of any commercial or financial relationships that could be construed as a potential conflict of interest.

Publisher's note

All claims expressed in this article are solely those of the authors and do not necessarily represent those of their affiliated organizations, or those of the publisher, the editors and the reviewers. Any product that may be evaluated in this article, or claim that may be made by its manufacturer, is not guaranteed or endorsed by the publisher.

Supplementary material

The Supplementary Material for this article can be found online at: https://www.frontiersin.org/articles/10.3389/feart.2024.1457377/full#supplementary-material

References

Adachi, M., Yamamoto, K., and Sugisaki, R. (1986). Hydrothermal chert and associated siliceous rocks from the northern Pacific their geological significance as indication od ocean ridge activity. *Sediment. Geol.* 47 (1-2), 125–148. doi:10.1016/0037-0738(86)90075-8

Adams, D. D., Hurtgen, M. T., and Sageman, B. B. (2010). Volcanic triggering of a biogeochemical cascade during oceanic anoxic event 2. *Nat. Geosci.* 3 (3), 201–204. doi:10.1038/ngeo743

Algeo, T. J., Chao, L., Johannesson, K., Algeo, T. J., Dickson, A. J., Morford, J. L., et al. (2020). Redox classification and calibration of redox thresholds in sedimentary systems. *Geochimica cosmochimica acta* 287, 8–26. doi:10.1016/j.gca.2020.01.055

Algeo, T. J., and Ingall, E. (2007). Sedimentary Corg:P ratios, paleocean ventilation, and Phanerozoic atmospheric pO2. *Palaeogeogr. Palaeoclimatol. Palaeoecol.* 256 (3-4), 130–155. doi:10.1016/j.palaeo.2007.02.029

Algeo, T. J., and Lyons, T. W. (2006). Mo-total organic carbon covariation in modern anoxic marine environments: implications for analysis of paleoredox and paleohydrographic conditions. *Paleoceanography* 21 (1), A1016. doi:10.1029/2004pa001112

Algeo, T. J., and Maynard, J. B. (2004). Trace-element behavior and redox facies in core shales of Upper Pennsylvanian Kansas-type cyclothems. *Chem. Geol.* 206 (3-4), 289–318. doi:10.1016/j.chemgeo.2003.12.009

Algeo, T. J., and Rowe, H. (2012). Paleoceanographic applications of trace-metal concentration data. *Chem. Geol.* 324-325 (324), 6–18. doi:10.1016/j.chemgeo.2011.09.002

Algeo, T. J., and Tribovillard, N. (2009). Environmental analysis of paleoceanographic systems based on molybdenum–uranium covariation. *Chem. Geol.* 268 (3-4), 211–225. doi:10.1016/j.chemgeo.2009.09.001

Calvert, S. E., and Pedersen, T. F. (1993). Geochemistry of Recent oxic and anoxic marine sediments: implications for the geological record. *Mar. Geol.* 113 (1), 67–88. doi:10.1016/0025-3227(93)90150-t

Canfield, D. E. (1994). Factors influencing organic carbon preservation in marine sediments. *Chem. Geol.* 114 (3), 315–329. doi:10.1016/0009-2541(94)90061-2

Cao, Q., Jiang, K., Wen, Z. T., Wang, X. Z., Qi, M. H., and Yin, Z. S. (2021). Characteristics of organic matter pores and the relationship with current pressure system of lower silurian Longmaxi shales in dingshan field, southern sichuan, China. *Geofluids* 2021, 1–15. doi:10.1155/2021/9967479

Chen, X., Rong, J. Y., Li, X., and Boucot, A. J. (2004). Facies patterns and geography of the Yangtze region, south China, through the ordovician and silurian transition. *Palaeogeogr. Palaeoclimatol. Palaeoecol.* 204 (3-4), 353–372. doi:10.1016/s0031-0182(03)00736-3

Demaison, G. J., and Moore, G. T. (1980). Anoxic environments and oil source bed genesis. *Org. Geochem.* 2 (1), 9–31. doi:10.1016/0146-6380(80)90017-0

Feng, Y., Xiao, X. M., Gao, P., Hu, D. F., Liu, R. B., Li, G., et al. (2024). Water distribution in pore systems and its influences on gas-bearing property of deep shale: a case study of the Longmaxi Formation in the Luzhou area, southern Sichuan Basin. *Mar. Petroleum Geol.* 163, 106805. doi:10.1016/j.marpetgeo.2024.106805

Feng, Y., Xiao, X. M., Gao, P., Wang, E. Z., Hu, D. F., Liu, R. B., et al. (2023a). Restoration of sedimentary environment and geochemical features of deep marine Longmaxi shale and its significance for shale gas: a case study of the Dingshan area in the Sichuan Basin, South China. *Mar. Petroleum Geol.* 151, 106186. doi:10.1016/j.marpetgeo.2023.106186

Feng, Y., Xiao, X. M., Wang, E. Z., Gao, P., Lu, C. G., and Li, G. (2023b). Gas storage in shale pore system: a review of the mechanism, control and assessment. *Petroleum Sci.* 20 (5), 2605–2636. doi:10.1016/j.petsci.2023.05.012

Feng, Y., Xiao, X. M., Wang, E. Z., Sun, J., and Gao, P. (2021). Oil retention in shales: a review of the mechanism, controls and assessment. *Front. Earth Sci.* 9, 710. doi:10.3389/feart.2021.720839

Froelich, P. N., Klinkhammer, G. P., Bender, M. L., Luedtke, N. A., Heath, G. R., Cullen, D., et al. (1979). Early oxidation of organic matter in pelagic sediments of the eastern equatorial Atlantic: suboxic diagenesis. *Geochimica Cosmochimica Acta* 43 (7), 1075–1090. doi:10.1016/0016-7037(79)90095-4

Gao, P., Xiao, X. M., Hu, D. F., Liu, R. B., Li, F., Zhou, Q., et al. (2022). Gas in place and its controlling factors of deep shale of the Wufeng-Longmaxi Formations in the Dingshan area, Sichuan Basin. *Front. Earth Sci.* 17 (1), 322–336. doi:10.1007/s11707-021-0966-5

Gao, P., Xiao, X. M., Hu, D. F., Lash, G. G., Liu, R. B., Cai, Y. D., et al. (2022). Effect of silica diagenesis on porosity evolution of deep gas shale reservoir of the Lower Paleozoic Wufeng-Longmaxi formations, Sichuan Basin. *Front. Earth Sci.Mar. Pet. Geol.* 145, 105873. doi:10.1016/j.marpetgeo.2022.105873

Gromet, L. P., Dymek, R. F., Haskin, L. A., and Korotev, R. L. (1984). The "North American shale composite"; its compilation, major and trace element

characteristics. *Geochimica cosmochimica acta* 48 (12), 2469–2482. doi:10.1016/0016-7037(84)90298-9

Guo, X. S., Hu, D. F., Huang, R. C., Wei, Z. H., Duan, J. B., Wei, X. F., et al. (2020). Deep and ultra-deep natural gas exploration in the Sichuan Basin: progress and prospect. *Nat. Gas. Ind.* 40 (05), 419–432. (In Chinese with English abstract). doi:10.1016/j.ngib.2020.05.001

He, X. H., Zhao, J. X., Zhou, R. J., Feng, Y. X., Leonard, N., Li, F., et al. (2022). The distribution and substitution mechanism of trace elements in cassiterites: constraints from LA-ICP-MS U-Pb dating, elemental mapping and *in situ* trace element analyses of the Gejiu tin polymetallic deposit, SW China. *Chem. Geol.* 609, 121063. doi:10.1016/j.chemgeo.2022.121063

He, Z. L., Nie, H. K., and Jiang, T. X. (2021). Challenges and countermeasures of effective development with large scale of deep shale gas in Sichuan Basin. *Petroleum Reserv. Eval. Dev.* 11 (2), 135–145. (In Chinese with English abstract). doi:10.13809/j.cnki.cn32-1825/te.2021.02.001

Hu, T., Jiang, F. J., Pang, X. Q., Liu, Y., Wu, G. Y., Zhou, K., et al. (2024). Identification and evaluation of shale oil micro-migration and its petroleum geological significance. *Petroleum Explor. Dev.* 51 (1), 127–140. doi:10.1016/s1876-3804(24)60010-8

Huang, W. M., Liu, S. G., Xu, G. S., Wang, G. Z., Ma, W. X., Zhang, C. J., et al. (2011). Characteristics of paleo oil pools from Sinian to Lower Paleozoic in southeastern margin of Sichuan basin. *Geol. Rev.* 57 (2), 285–299. (In Chinese with English abstract).

Jin, C. S., Li, C., Algeo, T. J., Wu, S. Y., Cheng, M., Zhang, Z. H., et al. (2020a). Controls on organic matter accumulation on the early-Cambrian western Yangtze Platform, South China. *Mar. Petroleum Geol.* 111, 75–87. doi:10.1016/j.marpetgeo.2019.08.005

Jin, C. S., Liao, Z. W., and Tang, Y. J. (2020b). Sea-level changes control organic matter accumulation in the Longmaxi shales of southeastern Chongqing, China. *Mar. Petroleum Geol.* 119, 104478. doi:10.1016/j.marpetgeo.2020.104478

Jones, B., and Manning, D. A. C. (1994). Comparison of geochemical indices used for the interpretation of palaeoredox conditions in ancient mudstones. *Chem. Geol.* 111 (1-4), 111–129. doi:10.1016/0009-2541(94)90085-x

Khan, M. Z., Feng, Q. L., Zhang, K., and Guo, W. (2019). Biogenic silica and organic carbon fluxes provide evidence of enhanced marine productivity in the Upper Ordovician-Lower Silurian of South China. *Palaeogeogr. Palaeoclimatol. Palaeoecol.* 534, 109278. doi:10.1016/j.palaeo.2019.109278

Larry, A. H., Thomas, R. W., Fred, A. F., Kenneth, A. C., Curtis, R. K., and Mary, A. (1966). Rare earths in sediments. *Geophys. Res.* 71 (24), 6091–6105. doi:10.1029/jz071i024p06091

Li, H. X., Liu, B., Liu, X. Z., Meng, L. N., Cheng, L. J., and Wang, H. X. (2019). Mineralogy and inorganic geochemistry of the Es4 shales of the damintun sag, northeast of the bohai bay basin: implication for depositional environment. *Mar. Petroleum Geol.* 110, 886–900. doi:10.1016/j.marpetgeo.2019.09.002

Li, Y. F., Zhang, T. W., Ellis, G. S., and Shao, D. Y. (2017). Depositional environment and organic matter accumulation of upper ordovician-lower silurian marine shale in the upper Yangtze Platform, south China. *Palaeogeogr. Palaeoclimatol. Palaeoecol.* 466, 252–264. doi:10.1016/j.palaeo.2016.11.037

Liu, B., Bechtel, A., Sachsenhofer, R. F., Gross, D., Gratzer, R., and Chen, X. (2017). Depositional environment of oil shale within the second member of permian lucaogou formation in the santanghu basin, northwest China. *Int. J. Coal Geol.* 175, 10–25. doi:10.1016/j.coal.2017.03.011

Liu, B., Sun, J. H., Zhang, Y. Q., He, J. L., Fu, X. F., Yang, L., et al. (2021). Reservoir space and enrichment model of shale oil in the first member of Cretaceous Qingshankou Formation in the Changling Sag, southern Songliao Basin, NE China. *Petroleum Explor. Dev.* 48 (03), 608–624. doi:10.1016/s1876-3804(21)60049-6

Liu, S. G., Yang, Y., Deng, B., Zhong, Y., Wen, L., Sun, W., et al. (2021). Tectonic evolution of the Sichuan Basin, southwest China. *Earth-science Rev.* 213, 103470. doi:10.1016/j.earscirev.2020.103470

Lu, C. G., Gao, P., Tiong, R. L. K., Feng, Y., Li, G., Meng, G. M., et al. (2024). Geochemical constraints and astronomical forcing on organic matter accumulation of marine-continental transitional shale deposits in the qinshui basin during the carboniferous-permian transition. *ACS Earth Space Chem.* 8 (3), 616–629. doi:10.1021/acsearthspacechem.3c00372

Lu, C. G., Xiao, X. M., Gai, H. F., Feng, Y., Li, G., Meng, G. M., et al. (2023). Nanopore structure characteristics and evolution of type III kerogen in marine-continental transitional shales from the Qinshui basin, northern China. *Geoenergy Sci. Eng.* 221, 211413. doi:10.1016/j.geoen.2022.211413

Lu, Z. Y., He, Z. L., Yu, C., Ye, X., Li, D. H., Du, W., et al. (2021). Characteristics of shale gas enrichment in tectonically complex regions-A case study of the Wufeng-Longmaxi Formations of Lower Paleozoic in southeastern Sichuan Basin. *Oil Gas Geol.* 42 (01), 86–97. (In Chinese with English abstract).

Luo, Q. Y., Zhong, N. N., Wang, Y. N., Zhang, Y. Q., Qin, J., Qi, L., et al. (2013). Geochemistry of mesoproterozoic hongshuizhuang formation shales inNorthern North

China:lmplications for provenance and source weathering. *Acta Geol. Sin.* 87 (12), 1913–1921. (In Chinese with English abstract).

Ma, X. H., Wang, H. Y., Zhou, S. W., Shi, Z. S., and Zhang, L. F. (2021). Deep shale gas in China: geological characteristics and development strategies. *Energy Rep.* 7, 1903–1914. doi:10.1016/j.egyr.2021.03.043

Ma, X. H., Xie, J., Yong, R., and Zhu, Y. Q. (2020). Geological characteristics and high production control factors of shale gas reservoirs in Silurian Longmaxi Formation, southern Sichuan Basin, SW China. *Petroleum Explor. Dev.* 47 (5), 901–915. doi:10.1016/s1876-3804(20)60105-7

McLennan, S. M. (2001). Relationships between the trace element composition of sedimentary rocks and upper continental crust. *Geochem. Geophys. geosystems* 2 (4), 1021. doi:10.1029/2000gc000109

McLennan, S. M., Hemming, S., McDaniel, D. K., Hanson, G. N., Johnsson, M. J., and Basu, A. (1993). Geochemical approaches to sedimentation, provenance, and tectonics. *Geol. Soc. Am. Special Pap.* 284, 21–40. doi:10.1130/spe284-p21

Meng, G. M., Li, T. F., Gai, H. F., and Xiao, X. M. (2022). Pore characteristics and gas preservation of the lower cambrian shale in a strongly deformed zone, northern chongqing, China. *Energies* 15 (8), 2956. doi:10.3390/en15082956

Meng, G. M., Gai, H. F., Yang, X. M., Gao, P., Zhou, Q., Lu, C. G., et al. (2024). Occurrence and maturation transformation of organic and inorganic nitrogen in the Lower Cambrian shelf–slope facies shale: Implications for overmature N_2-rich shale reservoirs in Southern China. *Mar. Pet. Geol.* 168, 107011. doi:10.1016/j.marpetgeo.2024.107011

Nesbitt, H. W., and Young, G. M. (1982). Early Proterozoic climates and plate motions inferred from major element chemistry of lutites. *Nature* 299 (5885), 715–717. doi:10.1038/299715a0

Nesbitt, H. W., and Young, G. M. (1989). Formation and diagenesis of weathering profiles. *Geology* 97 (2), 129–147. doi:10.1086/629290

Nesbitt, H. W., and Young, G. M. (1996). Petrogenesis of sediments in the absence of chemical weathering: effects of abrasion and sorting on bulk composition and mineralogy. *Sedimentology* 43 (2), 341–358. doi:10.1046/j.1365-3091.1996.d01-12.x

Nie, H. K., Jin, Z. J., Li, P., Jay Katz, B., Dang, W., Liu, Q. Y., et al. (2023). Deep shale gas in the Ordovician-Silurian Wufeng-Longmaxi formations of the Sichuan Basin, SW China: insights from reservoir characteristics, preservation conditions and development strategies. *J. Asian Earth Sci.* 244, 105521. doi:10.1016/j.jseaes.2022.105521

Pan, Y. S., Huang, Z. L., Li, T. J., Guo, X. B., Xu, X. F., and Chen, X. (2020). Environmental response to volcanic activity and its effect on organic matter enrichment in the permian lucaogou formation of the malang sag, santanghu basin, northwest China. *Palaeogeogr. Palaeoclimatol. Palaeoecol.* 560 (0), 110024. doi:10.1016/j.palaeo.2020.110024

Pedersen, T. F., and Calvert, S. E. (1990). Anoxia vs. Productivity what controls the formation of organic-carbon-rich sediments and sedimentary rocks. *AAPG Bull.* 74 (04), 454–466. doi:10.1306/0c9b232b-1710-11d7-8645000102c1865d

Peng, J. W., Hu, Z. Q., Feng, D. J., and Wang, Q. R. (2023). Variations of organic matter content and type within the sequence stratigraphic framework of the lacustrine deep-water Dongyuemiao formation, Sichuan Basin, Western China. *Mar. Petroleum Geol.* 149, 106104. doi:10.1016/j.marpetgeo.2023.106104

Piper, D. Z., Perkins, R. B., Schultz, R. B., and Rimmer, S. N. (2004). A modern vs. Permian black shale; the hydrography, primary productivity, and water-column chemistry of deposition. *Chem. Geol.* 206 (3-4), 177–197. doi:10.1016/j.chemgeo.2003.12.006

Qiu, Z., Lu, B., Chen, Z. H., Zhang, R., Dong, D. Z., Wang, H. Y., et al. (2019). Discussion of the relationship between volcanic ash layers and organic enrichment of black shale: a case study of the wufeng-longmaxi gas shales in the Sichuan Basin. *Acta Sedimentol. Sin.* 37 (06), 1296–1308. (In Chinese with English abstract). doi:10.14027/j.issn.1000-0550.2019.088

Shen, J. J., Wang, Y. M., Li, H., Ji, Y. B., Qiu, Z., Wang, P. W., et al. (2023). Relationship between degree of water retention and enrichment of shale organic matter during the Ordovician-Silurian transition in western Hubei. *Acta Pet. Sin.* 44 (10), 1599–1611. (In Chinese with English abstract).

Shu, Z. G., and Wang, J. (2021). Geological characteristics analysis and favorable area optimization of upper shale gas reservoir of Jiaoshiba block in Fuling Gas Field, Sichuan Basin. *Petroleum Geol. Exp.* 43 (1), 34–45. (In Chinese with English abstract). doi:10.11781/sysydz202101034

Shu, Z. H., Fang, D. L., Zheng, A. W., Liu, C., Liu, L., Ji, J., et al. (2020). Geological characteristics and development potential of upper shale gas reservoirs of No.1 member of Longmaxi Formation in Jiaoshiba area, Sichuan Basin. *Nat. Gas. Geosci.* 31 (3), 393–401. (In Chinese with English abstract). doi:10.11764/j.issn.1672-1926.2019.12.016

Steenbergh, A. K., Bodelier, P. L. E., Hoogveld, H. L., Slomp, C. P., and Laanbroek, H. J. (2011). Phosphatases relieve carbon limitation of microbial activity in Baltic Sea sediments along a redox-gradient. *Limnol. Oceanogr.* 56 (6), 2018–2026. doi:10.4319/lo.2011.56.6.2018

Tan, J. Q., Wang, Z. H., Wang, W. H., Hilton, J., Guo, J. H., and Wang, X. K. (2021). Depositional environment and hydrothermal controls on organic matter enrichment in the lower Cambrian Niutitang shale, southern China. *AAPG Bull.* 105 (7), 1329–1356. doi:10.1306/12222018196

Taylor, S. R., and McLennan, S. M. (1985). The continental crust its composition and evolution. *Geol. Mag.* 122 (6), 673–674. doi:10.1017/s0016756800032167

Tribovillard, N., Algeo, T. J., Lyons, T., and Riboulleau, A. (2006). Trace metals as paleoredox and paleoproductivity proxies: an update. *Chem. Geol.* 232 (1-2), 12–32. doi:10.1016/j.chemgeo.2006.02.012

Vink, S., Chambers, R. M., and Smith, S. V. (1997). Distribution of phosphorus in sediments from tomales bay, California. *Mar. Geol.* 139 (1), 157–179. doi:10.1016/s0025-3227(96)00109-0

Walker, W. J., Cronan, C. S., and Patterson, H. H. (1988). A kinetic study of aluminum adsorption by aluminosilicate clay minerals. *Geochimica cosmochimica acta* 52 (1), 55–62. doi:10.1016/0016-7037(88)90056-7

Wang, E. Z., Feng, Y., Guo, T. L., and Li, M. W. (2022a). Oil content and resource quality evaluation methods for lacustrine shale: a review and a novel three-dimensional quality evaluation model. *Earth-Science Rev.* 232, 104134. doi:10.1016/j.earscirev.2022.104134

Wang, E. Z., Feng, Y., Guo, T. L., Li, M. W., Xiong, L., Lash, G. G., et al. (2023). Sedimentary differentiation triggered by the Toarcian Oceanic Anoxic Event and formation of lacustrine shale oil reservoirs: organic matter accumulation and pore system evolution of the Early Jurassic sedimentary succession, Sichuan Basin, China. *J. Asian Earth Sci.* 256, 105825. doi:10.1016/j.jseaes.2023.105825

Wang, H. Y., Zhou, S. W., Li, S. S., Zhao, M., and Zhu, T. (2022b). Comprehensive characterization and evaluation of deep shales from Wufeng-Longmaxi Formation by LF-NMR technology. *Unconv. Resour.* 2, 1–11. doi:10.1016/j.uncres.2022.05.001

Wang, R. Y., Ding, W. L., Zhang, Y. Q., Wang, Z., Wang, X. H., He, J. H., et al. (2016). Analysis of developmental characteristics and dominant factors of fractures in Lower Cambrian marine shale reservoirs: a case study of Niutitang formation in Cen'gong block, southern China. *J. Petroleum Sci. Eng.* 138, 31–49. doi:10.1016/j.petrol.2015.12.004

Wang, R. Y., Hu, Z. Q., Long, S. X., Liu, G. X., Zhao, J. H., Dong, L., et al. (2019). Differential characteristics of the Upper Ordovician-Lower Silurian Wufeng-Longmaxi shale reservoir and its implications for exploration and development of shale gas in/around the Sichuan Basin. *Acta Geol. Sin.* 93 (3), 520–535. doi:10.1111/1755-6724.13875

Wang, R. Y., Nie, H. K., Hu, Z. Q., Liu, G. X., Xi, B. B., and Liu, W. X. (2020). Controlling effect of pressure evolution on shale gas reservoirs: a case study of the Wufeng-Longmaxi Formation in the Sichuan Basin. *Nat. Gas. Ind.* 40 (10), 1–11.

Wedepohl, K. H. (1971). Environmental influences on the chemical composition of shales and clays. *Phys. Chem. earth* 8, 307–333. doi:10.1016/0079-1946(71)90020-6

Wei, X. F., Liu, Z. J., Wang, Q., Wei, F. B., and Yuan, T. (2020). Analysis and thinking of the difference of Wufeng-Longmaxi shale gas enrichment conditions between Dingshan and Jiaoshiba areas in southeastern Sichuan Basin. *Nat. Gas. Geosci.* 31 (8), 1041–1051. (In Chinese with English abstract).

Wu, L. Y., Lu, Y. C., Jiang, S., Liu, X. F., and He, G. S. (2018). Effects of volcanic activities in ordovician wufeng-silurian Longmaxi period on organic-rich shale in the upper Yangtze area, south China. *Petroleum Explor. Dev.* 45 (05), 862–872. (In Chinese with English abstract). doi:10.1016/s1876-3804(18)30089-2

Wu, Z. Y., Zhao, X. Z., Wang, E. Z., Pu, X. G., Lash, G., Han, W. Z., et al. (2021). Sedimentary environment and organic enrichment mechanisms of lacustrine shale: a case study of the paleogene shahejie formation, qikou sag, bohai bay basin. *Palaeogeogr. Palaeoclimatol. Palaeoecol.* 573, 110404. doi:10.1016/j.palaeo.2021.110404

Yang, P., Wu, G. H., Nuriel, P., Nguyen, A. D., Chen, Y. Q., Yang, S., et al. (2021). *In situ* LA-ICPMS U-Pb dating and geochemical characterization of fault-zone calcite in the central Tarim Basin, northwest China: implications for fluid circulation and fault reactivation. *Chem. Geol.* 568, 120125. doi:10.1016/j.chemgeo.2021.120125

Yang, S. C., Hu, W. X., Fan, J. X., and Deng, Y. Y. (2022). New geochemical identification fingerprints of volcanism during the Ordovician-Silurian transition and its implications for biological and environmental evolution. *Earth-Science Rev.* 228, 104016. doi:10.1016/j.earscirev.2022.104016

Zeng, S. Q., Wang, J., Fu, X. G., Chen, W. B., Feng, X. L., Wang, D., et al. (2015). Geochemical characteristics, redox conditions, and organic matter accumulation of marine oil shale from the Changliang Mountain area, northern Tibet, China. *Mar. Petroleum Geol.* 64 (0), 203–221. doi:10.1016/j.marpetgeo.2015.02.031

Zhang, P. Y., Wang, Y. L., Wei, Z. F., Wang, G., Zhang, T., He, W., et al. (2023). Influence of the Late Ordovician-Early Silurian paleoenvironment and related geological processes on the organic matter accumulation and carbon

isotope excursion. *Paleoceanogr. Paleoclimatology* 38 (7), e2023PA004628. doi:10.1029/2023pa004628

Zhang, P. Y., Wang, Y. L., Zhang, X. J., Wei, Z. F., Wang, G., Zhang, T., et al. (2022). Carbon, oxygen and strontium isotopic and elemental characteristics of the Cambrian Longwangmiao Formation in South China: paleoenvironmental significance and implications for carbon isotope excursions. *Gondwana Res.* 106, 174–190. doi:10.1016/j.gr.2022.01.008

Zheng, F. Z., Tang, X., Yuan, K., Lin, T., You, M. X., Niu, J. L., et al. (2022). Sedimentation models and development mechanisms of organic-rich shales of the lower carboniferous dawuba formation: a case study in the yaziluo rift trough, south of Guizhou province, southern China. *ACS Omega* 7 (33), 29054–29071. doi:10.1021/acsomega.2c02901

Zheng, Y. J., Liao, Y. H., Wang, J., Xiong, Y. Q., Wang, Y. P., and Peng, P. A. (2024). Factors controlling the heterogeneity of shale pore structure and shale gas production of the Wufeng–Longmaxi shales in the Dingshan plunging anticline of the Sichuan Basin, China. *Int. J. Coal Geol.* 282, 104434. doi:10.1016/j.coal.2023.104434

Zou, C. N., Zhao, Q., Cong, L. Z., Wang, H. Y., Shi, Z. S., Wu, J., et al. (2021). Development progress, potential and prospect of shale gas in China. *Nat. Gas. Ind.* 41 (01), 1–14. (In Chinese with English abstract). doi:10.3787/j.issn.1000-0976.2021.01.001

Zou, C. N., Zhu, R. K., Chen, Z. Q., Ogg, J. G., Wu, S. T., Dong, D. Z., et al. (2019). Organic-matter-rich shales of China. *Earth-Science Rev.* 189, 51–78. doi:10.1016/j.earscirev.2018.12.002